# Caspase-mediated nuclear pore complex trimming in cell differentiation and endoplasmic reticulum stress

Ukrae H. Cho[1, *] and Martin W. Hetzer[1, *]

[1]Molecular and Cell Biology Laboratory, Salk Institute for Biological Studies, La Jolla, CA 92037, USA

*Correspondence should be addressed to
U.H.C (ucho@salk.edu) or M.W.H (hetzer@salk.edu)

## Introductory Paragraph

During programmed cell death, caspases degrade 7 out of ~30 nucleoporins (Nups) to irreversibly demolish the nuclear pore complex (NPC)[1]. However, for poorly understood reasons, caspases are also activated in differentiating cells in a non-apoptotic manner[2,3]. Here, we describe reversible, caspase-mediated NPC "trimming" during early myogenesis. We find that sublethal levels of caspases selectively proteolyze 4 peripheral Nups, Nup358, Nup214, Nup153, and Tpr, resulting in the transient block of nuclear export pathways. Several nuclear export signal (NES)-containing focal adhesion proteins concomitantly accumulate in the nucleus where they function as transcription cofactors[4]. We show that one such protein, FAK (focal adhesion kinase), drives a global reconfiguration of MBD2 (methyl CpG binding domain protein 2)-mediated genome regulation. We also observe caspase-mediated NPC trimming during neurogenesis and endoplasmic reticulum (ER) stress. Our results illustrate that the NPC can be proteolytically regulated in response to non-apoptotic cues, and call for a reassessment of the death-centric view of caspases.

Caspase-mediated NPC proteolysis has been extensively studied in apoptotic cells[1]. It enables rapid nuclear translocation of pro-apoptotic proteins such as cytochrome C, caspase-3, apoptosis-inducing factors, and macrophage migration inhibitory factor[5-8]. However, it remains unknown whether NPCs are targeted by caspases in differentiating cells where their activation is sublethal and transient. We therefore assessed Nup degradation in C2C12 cells undergoing myoblast-to-myotube transition[9]. Strikingly, during the first few days of myogenesis, 4 peripheral Nups, Nup358, Nup214, Nup153, and Tpr, were reversibly and completely degraded in a caspase-dependent manner (**Fig. 1a** and **Extended Data Fig. 1a**). Interestingly, Nup96 and Nup93, which form NPC scaffold and are cleaved by caspases during apoptosis[1], remained intact (**Fig. 1a**). This is in line with our previous report that described the persistence of the same Nup96 and Nup93 copies through the course of differentiation[10]. Hence, from the NPC quaternary structure perspective, caspases trim the cytoplasmic filaments and nuclear basket while sparing the membrane-traversing Nups, allowing rapid re-assembly of functional NPCs upon their quenching (**Fig. 1b**). Of note, although calpains, another class of proteases that are activated during myogenesis[11], can proteolyze Nups like caspases[12], calpain inhibition delayed but did not prevent Nup degradation in differentiating C2C12 cells (**Extended Data Fig. 1a**).

The removal of four peripheral Nups has been shown to block nuclear export and cause nuclear accumulation of RNAs and NES-containing proteins[13-16]. We assessed mRNA export by combining nuclear isolation and oligo(dT) bead-based poly(A)$^+$ RNA purification (**Fig. 1c**). The

nuclear-to-total mRNA ratio surges from 34% to 60% during differentiation, indicating an impairment in nuclear export. We then asked if the localization of α-tubulin is affected (**Fig. 1d**). In normal conditions, even though tubulin monomers can cross the NPC passive permeability barrier, they appear completely cytoplasmic due to multiple NESs[17]. Consistently, one day after switching to differentiation medium, when caspase activity is at its peak and NPCs are partially disintegrated, α-tubulin was detectable in the nucleus. We further checked if focal adhesion proteins with genome-regulatory functions accumulate in the nucleus since they (1) contain one or more NESs and (2) are likely to be released to the cytoplasm by calpains in differentiating C2C12 cells[11] and enter the nucleus by passive diffusion or by hitchhiking on their respective partner transcription factors[4]. Out of five focal adhesion proteins that we examined (**Supplementary Table 1**), four (Hic-5, zyxin, paxillin, and FAK) transiently became nuclear during myogenic differentiation (**Fig. 1e**). To confirm that the nuclear accumulation of NES-containing focal adhesion proteins is a consequence of caspase-mediated NPC trimming, we blocked the proteolysis of Nups using a pan-caspase inhibitor, Q-VD-OPh (**Fig. 1f**). The nuclear entrapment of Hic-5, zyxin, paxillin, and FAK was notably suppressed, albeit not fully. The residues can be ascribed to forced import by partner transcription factors – for example, MBD2 for FAK[18] and nuclear receptors for Hic-5[19]. In short, differentiation-associated caspase activity blocks nuclear export and leads to the nuclear retention of NES-containing proteins.

While characterizing the caspase-mediated nuclear export shutdown, we identified two potential mechanisms that can support cell survival during this time window: (1) Nuclear FAK is known to promote p53 degradation during apoptotic conditions to increase the chance of cell survival[20], and we observed a similar p53 reduction coinciding with the nuclear retention of FAK in differentiating C2C12 cells (**Fig. 1f**); (2) The distribution of housekeeping gene RNAs with extended half-lives, 18S ribosomal RNA[21] and *Gapdh* transcript[22], remains unchanged by NPC breakdown (**Extended Data Fig. 1b**), allowing cells to continuously synthesize essential proteins over the course of myogenesis.

Among the four focal adhesion proteins that accumulate in the nucleus, FAK is particularly intriguing in that it can facilitate cell survival, migration, cytoskeleton remodeling, and gene (de)activation, all of which are required for cell differentiation[23]. For example, FAK binds and removes MBD2 – the main component of the gene-repressive NuRD (nucleosome remodeling and deacetylation) complex[24] – from methylated CpGs within the *Myog* promoter[18]. We speculated that the FAK-mediated MBD2 dissociation during myotube formation is not limited to *Myog* and is rather a genome-wide phenomenon. To test this, we employed CUT&RUN-sequencing[25] and examined how MBD2-binding landscape changes in differentiating C2C12 cells

(**Fig. 2a** and **Extended Data Fig. 2a**). In confluent myoblasts, there were 9791 MBD2-bound loci, but the number plummeted to 354 in 24 hours as expected. Of note, MBD2 protein level stays constant during this time window, although it is eventually reduced in mature myotubes (**Fig. 2b** and **Extended Data Fig. 2b**). After the completion of myogenic differentiation, only few tens of MBD2 interacting sites were identifiable. We thus conclude that MBD2 genome-binding rapidly dissolves during myogenesis.

MBD2 overexpression has been reported to cause heterochromatin clustering like its cousin, MeCP2 (methyl CpG-binding protein 2)[18,26]. However, we find that at the endogenous levels, only MeCP2 localizes to the chromocenters in myotubes and that MBD2 does not spatially overlap with MeCP2 (**Extended Data Fig. 2c and d**), indicating that the two methyl CpG-binding proteins carry out disparate tasks. To better understand MBD2 in the context of myogenesis, we further analyzed MBD2 CUT&RUN-sequencing data from confluent myoblasts (Day 0 in **Fig. 2a**). About a quarter of the peaks were in promoters, roughly one-third in introns, and another one-third in distal intergenic regions (**Extended Data Fig. 3a**). Intense peaks were predominantly located within promoters (**Extended Data Fig. 3b**), and strikingly, the gene ontology (GO) term analysis revealed that MBD2 primarily targets the promoter of the genes that have a direct link to myogenic differentiation, with actin cytoskeleton organization (GO: 0030036) and muscle structure development (GO: 0061061) genes being the top 2 categories (**Fig. 2c**, see **Extended Data Fig. 3c** for the GO analysis of the entire MBD2 target genes). *Mylpf* (myosin light chain, phosphorylatable, fast skeletal muscle), whose mutation recently has been shown to cause a familial segmental amyoplasia[27], is one noteworthy example (**Extended Data Fig. 3d**). In short, MBD2 binds, and potentially regulates, cell identity genes in muscle cells.

We then evaluated how transcription changes after MBD2 is removed from the promoters. Considering that most MBD2-bound promoters are already tri-methylated at Histone H3 lysine 4 in myoblasts (**Extended Data Fig. 4a and b**), we expected that MBD2-target genes would be upregulated after MBD2 dissociation, or the loss of the NuRD complex. However, RNA-sequencing revealed that out of 1508 genes, only 218 exhibit >2-fold increase in transcript levels whereas 336 show >2-fold decrease (**Fig. 2d** and **Extended Data Fig. 4c**). It is possible that other gene repressing mechanisms – such as non-MBD2 methyl CpG binding proteins, heterochromatin reorganization, and gene-specific repressors – are taking over during myogenesis.

To summarize, caspase-mediated NPC trimming coincides with nuclear sequestration of NES-containing proteins, which can be transformative as in the case of FAK or inconsequential (presumably) as in the case of $\alpha$-tubulin (**Fig. 2e**). Our finding agrees with a previous

immunofluorescence-based study[28] that described (1) the transient nuclear translocation of an NES-containing E3 ligase Nedd4 during myogenesis, which causes Pax7 degradation, and (2) the 2- to 3-fold enhancement of myogenin activation in the presence of leptomycin b, an exportin-1 inhibitor. We validated that a partial dose of leptomycin b increases myogenin at 24 hours post-differentiation (**Extended Data Fig. 4d**).

We then sought to determine how caspases are sublethally activated during myogenic differentiation. We surmised that caspase-inhibiting proteins could be downregulated to facilitate caspase activation. Among eight inhibitors of apoptosis proteins (IAPs), cIAP-1/2, XIAP, and survivin are most extensively studied and considered the major caspase counteractors[29]. The XIAP and survivin can be regulated by the Notch signaling pathway[30,31], which plays a key role in myogenesis. We monitored the expression of these IAPs over the course of differentiation in the absence or presence of DAPT, a γ-secretase inhibitor that blocks the release of the Notch intracellular domain (**Fig. 3a**). We noted two intriguing points. First, survivin was dramatically downregulated in the first 24 hours. Second, none of the examined IAP levels were affected by DAPT treatment. This indicates that Notch signaling does not control these proteins during myogenesis.

To validate that survivin downregulation amplifies caspase-3 activity, we incubated HCT116 cells with 1541B and/or YM155, chemicals that catalyze the proteolytic processing of procaspase-3[32] or inhibits survivin transcription in cancer cells[33], respectively (**Extended Data Fig. 5a**). 1541B gave rise to the active form of caspase-3 and induced the degradation of Tpr, Nup153, and PARP (poly (ADP-ribose) polymerase) as well as cIAP-1 and XIAP[34,35], all of which were accelerated and enhanced when 1541B was used in combination with YM155. (YM155 alone decreases survivin, but not cIAP-1/2 and XIAP, and does not activate caspase-3.) This suggests that survivin suppression can potentiate caspase-3 activity.

We also discovered that calpain inhibition delays, but does not prevent, the activation of caspase-3 and -12 and the degradation of peripheral Nups and PARP (**Extended Data Fig. 1a** and **Extended Data Fig. 5b**). This signifies that, while calpains are upstream of caspases, there is another caspase activation pathway. Given that unfolded protein response is triggered in differentiating C2C12 cells[36], we surmise that procaspase-12 is processed by IRE1 and TRAF2 and converts procaspase-3 to its active form (p17) as in ER stress conditions[37,38].

Next, we examined the relationship between caspase activation and myogenin, the main driver of myotube formation (**Fig. 3b**). To this end, we generated a C2C12 stable cell line that expresses green fluorescent protein (GFP)-fused myogenin in a doxycycline-dependent manner. Exogenous myogenin accelerated by a day the upregulation of myosin heavy chain (MHC), and

more importantly, the reduction of active caspase-3, suggesting that a caspase-quenching pathway exists and is activated once myoblasts pass a certain differentiation stage. Caspase inhibition prevented the expression of myogenin, and thus MHC, as previously reported[9]. We then asked whether differentiation blockage by caspase inhibition can be overridden by exogenous myogenin (**Fig. 3b**). Doxycycline-induced expression of GFP-myogenin enabled the upregulation of both endogenous myogenin and MHC even when a pan-caspase inhibitor was present. (The myotubes, however, appeared not as robust as the ones formed in the presence of DMSO or doxycycline alone; data not shown). This demonstrates that the key function of caspases is to upregulate myogenin, the master regulator, and that the proteolyses of other targets are ancillary events that render cells amenable for differentiation.

Finally, we explored whether the proteolytic processing of caspase-3 is linked to the phosphatase activity of calcineurin (**Fig. 3c**), as it is required for the nuclear translocation of NFAT (nuclear factor of activated T-cells) and the transcriptional activation of myogenin[39]. We differentiated C2C12 cells in the absence or presence of FK506, a macrolide that suppresses calcineurin activity, and found that the p17 form of caspase-3 arises even when FK506 is used at the highest dose and when myogenin upregulation is subdued. This result illustrates that the calcineurin/NFAT/myogenin pathway is orthogonal to the caspase/myogenin pathway. **Fig. 3d** summarizes our working model. Taken together, we have identified a new cascade – (1) caspase activation, (2) peripheral Nup degradation, (3) nuclear retention of NES-containing proteins – that regulates the expression of myogenin[24], Pax7[28], and other myogenesis-related genes (**Fig. 2e** and **Fig. 3d**).

To test that caspase-mediated NPC trimming is not a myogenesis-specific phenomenon, we differentiated H9 embryonic stem cell-derived neural precursor cells into mature, post-mitotic neurons, and looked into caspase-related events (**Fig. 4a**). As in myogenic differentiation, survivin is highly expressed in precursor cells but undetectable in mature neurons. cIAP-1/2 is modestly reduced while XIAP remains constant. The processing of caspase-3 to the p17 form and the proteolysis of Nup153 and PARP were observed concomitantly. In short, the same processes occur during neuronal differentiation, but over a longer duration.

We also tested whether partial NPC disintegration takes place during ER stress since the calpain/caspase activation pathway in unfolded protein response is similar to that in myogenesis (**Fig. 3d**). C2C12 myotubes, reserve cells, and myoblasts were treated with 1 μg/mL tunicamycin (**Fig. 4b**). Active caspase-3 arose in all three cell types and Tpr and Nup153 degradation was recognizable by 18 hours in C2C12 myoblasts and reserve cells; however, in myotubes, the two Nups were fully proteolyzed in less than 6 hours. The result can be attributed to the difference in

survivin and XIAP expression levels, both of which are lowest in myotubes at 0 hour. (Furthermore, XIAP in myotubes migrates faster than that in reserve cells or myoblasts during gel electrophoresis, possibly due to the dephosphorylation of Ser87, which is known to stabilize XIAP[40].) We conclude that NPC trimming occurs during ER stress at varying rates in different cell types. Of note, Nup93, a scaffold Nup, remained unaffected as in myogenesis, showing that it is better protected from caspases compared to peripheral Nups. Additionally, we tested whether low-level but sustained ER stress can induce the same phenotype in C2C12 myotubes (**Fig. 4c**). In fact, several myopathies involve chronic – rather than acute – ER stress and caspase activation[41]. We maintained differentiated C2C12 cells at low doses of tunicamycin (<50 ng/mL) for a week, and as in differentiating myoblasts (**Fig. 1a**) and acutely ER-stressed myotubes (**Fig. 4b**), major peripheral Nups were noticeably degraded while the breakdown of Nup93 was minimal. NPC trimming may contribute to cellular homeostasis loss in muscular diseases that accompany ER stress (**Fig. 4d**).

In summary, our study demonstrates that the NPC cytoplasmic filaments and nuclear basket are transiently removed by caspases in differentiating and ER-stressed cells. This process is distinct from terminal NPC destruction in apoptosis. Caspase-mediated NPC trimming is a reversible process that, for a set period during differentiation, impairs nuclear export. We found that during myogenesis, it is exploited to increase the nuclear levels of focal adhesion proteins that can double as transcription cofactors and to reconfigure the transcriptional profile of myoblasts. In addition, NPC trimming could reset NPC-genome interaction during cell differentiation. NPCs bind and regulate cell identity genes[42], and transient proteolysis of the nuclear basket can be an elegant reinitialization mechanism. During ER stress, the same phenomenon can potentially be utilized to curtail mRNA export, thereby reducing the protein synthesis/folding load in the ER. While we primarily focused on the NPC, the degradation of other caspase substrates might promote cell differentiation in their own ways. For example, caspases target several cytoskeletal proteins (e.g. αII-spectrin in **Fig. 1a**), which can accelerate cell morphological change. Proteolytic inactivation of transcription factors[43,44] and translation-related proteins can also be conducive for transcriptome and proteome turnover. Our findings support the idea that caspases initially evolved to change cell morphology, behavior, and identity, and that apoptosis is rather an extreme form of caspase-mediated cellular transformation[2,3].

**Acknowledgments**

We thank the members of the Hetzer lab and Jongmin Kim (Massachusetts General Hospital) for the critical reading of the manuscript; Kenneth Diffenderfer and Aimee Pankonin (Stem Cell Core Facility at the Salk Institute) for help with neurogenesis; Carol Marchetto and Fred Gage (the Salk Institute) for providing H9 embryonic stem cells. This work was supported by a Glenn Foundation for Medical Research Postdoctoral Fellowship in Aging Research (U.H.C.), the NOMIS foundation (M.W.H), and the National Institutes of Health (R01 NS096786 to M.W.H.).

**Author contributions**

U.H.C. performed experiments. U.H.C. and M.W.H. conceived the study and wrote the manuscript.

**Competing financial interests**

The authors declare no competing financial interests.

## References


1 Patre, M. *et al.* Caspases target only two architectural components within the core structure of the nuclear pore complex. *J Biol Chem* **281**, 1296-1304 (2006).

2 Connolly, P. F., Jager, R. & Fearnhead, H. O. New roles for old enzymes: killer caspases as the engine of cell behavior changes. *Front Physiol* **5**, 149 (2014).

3 Burgon, P. G. & Megeney, L. A. Caspase signaling, a conserved inductive cue for metazoan cell differentiation. *Semin Cell Dev Biol* **82**, 96-104 (2018).

4 Hervy, M., Hoffman, L. & Beckerle, M. C. From the membrane to the nucleus and back again: bifunctional focal adhesion proteins. *Curr Opin Cell Biol* **18**, 524-532 (2006).

5 Diaz-Moreno, I., Velazquez-Cruz, A., Curran-French, S., Diaz-Quintana, A. & De la Rosa, M. A. Nuclear cytochrome c - a mitochondrial visitor regulating damaged chromatin dynamics. *FEBS Lett* **592**, 172-178 (2018).

6 Bano, D. & Prehn, J. H. M. Apoptosis-Inducing Factor (AIF) in Physiology and Disease: The Tale of a Repented Natural Born Killer. *EBioMedicine* **30**, 29-37 (2018).

7 Kamada, S., Kikkawa, U., Tsujimoto, Y. & Hunter, T. Nuclear translocation of caspase-3 is dependent on its proteolytic activation and recognition of a substrate-like protein(s). *J Biol Chem* **280**, 857-860 (2005).

8 Wang, Y. *et al.* A nuclease that mediates cell death induced by DNA damage and poly(ADP-ribose) polymerase-1. *Science* **354**, aad6872 (2016).

9 Fernando, P., Kelly, J. F., Balazsi, K., Slack, R. S. & Megeney, L. A. Caspase 3 activity is required for skeletal muscle differentiation. *Proc Natl Acad Sci U S A* **99**, 11025-11030 (2002).

10 Toyama, B. H. *et al.* Visualization of long-lived proteins reveals age mosaicism within nuclei of postmitotic cells. *J Cell Biol* **218**, 433-444 (2019).

11 Louis, M., Zanou, N., Van Schoor, M. & Gailly, P. TRPC1 regulates skeletal myoblast migration and differentiation. *J Cell Sci* **121**, 3951-3959 (2008).

12 Bano, D. *et al.* Alteration of the nuclear pore complex in Ca(2+)-mediated cell death. *Cell Death Differ* **17**, 119-133 (2010).

13 Hutten, S. & Kehlenbach, R. H. Nup214 is required for CRM1-dependent nuclear protein export in vivo. *Mol Cell Biol* **26**, 6772-6785 (2006).

14 Ullman, K. S., Shah, S., Powers, M. A. & Forbes, D. J. The nucleoporin nup153 plays a critical role in multiple types of nuclear export. *Mol Biol Cell* **10**, 649-664 (1999).

15 Aksenova, V. *et al.* Nucleoporin TPR is an integral component of the TREX-2 mRNA export pathway. *Nat Commun* **11**, 4577 (2020).

16 Forler, D. *et al.* RanBP2/Nup358 provides a major binding site for NXF1-p15 dimers at the nuclear pore complex and functions in nuclear mRNA export. *Mol Cell Biol* **24**, 1155-1167 (2004).

17 Schwarzerova, K. *et al.* Tubulin is actively exported from the nucleus through the Exportin1/CRM1 pathway. *Sci Rep* **9**, 5725 (2019).

18 Luo, S. W. *et al.* Regulation of heterochromatin remodelling and myogenin expression during muscle differentiation by FAK interaction with MBD2. *EMBO J* **28**, 2568-2582 (2009).

19 Alpha, K. M., Xu, W. & Turner, C. E. Paxillin family of focal adhesion adaptor proteins and regulation of cancer cell invasion. *Int Rev Cell Mol Biol* **355**, 1-52 (2020).

20 Lim, S. T. *et al.* Nuclear FAK promotes cell proliferation and survival through FERM-enhanced p53 degradation. *Mol Cell* **29**, 9-22 (2008).

21 Yi, X., Tesmer, V. M., Savre-Train, I., Shay, J. W. & Wright, W. E. Both transcriptional and posttranscriptional mechanisms regulate human telomerase template RNA levels. *Mol Cell Biol* **19**, 3989-3997 (1999).

22 Lee, J. E., Lee, J. Y., Wilusz, J., Tian, B. & Wilusz, C. J. Systematic analysis of cis-elements in unstable mRNAs demonstrates that CUGBP1 is a key regulator of mRNA decay in muscle cells. *PLoS One* **5**, e11201 (2010).

23 Kleinschmidt, E. G. & Schlaepfer, D. D. Focal adhesion kinase signaling in unexpected places. *Curr Opin Cell Biol* **45**, 24-30 (2017).

24 Wood, K. H. & Zhou, Z. Emerging Molecular and Biological Functions of MBD2, a Reader of DNA Methylation. *Front Genet* **7**, 93 (2016).

25 Skene, P. J. & Henikoff, S. An efficient targeted nuclease strategy for high-resolution mapping of DNA binding sites. *eLife* **6** (2017).

26 Brero, A. *et al.* Methyl CpG-binding proteins induce large-scale chromatin reorganization during terminal differentiation. *J Cell Biol* **169**, 733-743 (2005).

27 Chong, J. X. *et al.* Mutations in *MYLPF* Cause a Novel Segmental Amyoplasia that Manifests as Distal Arthrogryposis. *Am J Hum Genet* **107**, 293-310 (2020).

28 Bustos, F. *et al.* NEDD4 Regulates PAX7 Levels Promoting Activation of the Differentiation Program in Skeletal Muscle Precursors. *Stem Cells* **33**, 3138-3151 (2015).

29 Srinivasula, S. M. & Ashwell, J. D. IAPs: what's in a name? *Mol Cell* **30**, 123-135 (2008).

30 Lee, C. W., Raskett, C. M., Prudovsky, I. & Altieri, D. C. Molecular dependence of estrogen receptor-negative breast cancer on a notch-survivin signaling axis. *Cancer Res* **68**, 5273-5281 (2008).

31 Liu, W. H., Hsiao, H. W., Tsou, W. I. & Lai, M. Z. Notch inhibits apoptosis by direct interference with XIAP ubiquitination and degradation. *EMBO J* **26**, 1660-1669 (2007).

32 Wolan, D. W., Zorn, J. A., Gray, D. C. & Wells, J. A. Small-molecule activators of a proenzyme. *Science* **326**, 853-858 (2009).

33 Nakahara, T. *et al.* YM155, a novel small-molecule survivin suppressant, induces regression of established human hormone-refractory prostate tumor xenografts. *Cancer Res* **67**, 8014-8021 (2007).

34 Guicciardi, M. E. *et al.* Cellular inhibitor of apoptosis 1 (cIAP-1) degradation by caspase 8 during TNF-related apoptosis-inducing ligand (TRAIL)-induced apoptosis. *Exp Cell Res* **317**, 107-116 (2011).

35 Hornle, M. *et al.* Caspase-3 cleaves XIAP in a positive feedback loop to sensitize melanoma cells to TRAIL-induced apoptosis. *Oncogene* **30**, 575-587 (2011).

36 Nakanishi, K., Sudo, T. & Morishima, N. Endoplasmic reticulum stress signaling transmitted by ATF6 mediates apoptosis during muscle development. *J Cell Biol* **169**, 555-560 (2005).

37 Morishima, N., Nakanishi, K., Takenouchi, H., Shibata, T. & Yasuhiko, Y. An endoplasmic reticulum stress-specific caspase cascade in apoptosis. Cytochrome c-independent activation of caspase-9 by caspase-12. *J Biol Chem* **277**, 34287-34294 (2002).

38 Yoneda, T. *et al.* Activation of caspase-12, an endoplastic reticulum (ER) resident caspase, through tumor necrosis factor receptor-associated factor 2-dependent mechanism in response to the ER stress. *J Biol Chem* **276**, 13935-13940 (2001).

39 Armand, A. S. *et al.* Cooperative synergy between NFAT and MyoD regulates myogenin expression and myogenesis. *J Biol Chem* **283**, 29004-29010 (2008).

40 Kato, K. *et al.* Protein kinase C stabilizes X-linked inhibitor of apoptosis protein (XIAP) through phosphorylation at Ser(87) to suppress apoptotic cell death. *Psychogeriatr* **11**, 90-97 (2011).

41 Afroze, D. & Kumar, A. ER stress in skeletal muscle remodeling and myopathies. *FEBS J* **286**, 379-398 (2019).

42 Cho, U. H. & Hetzer, M. W. Nuclear Periphery Takes Center Stage: The Role of Nuclear Pore Complexes in Cell Identity and Aging. *Neuron* **106**, 899-911 (2020).

43 Dick, S. A. *et al.* Caspase 3 cleavage of Pax7 inhibits self-renewal of satellite cells. *Proc Natl Acad Sci U S A* **112**, E5246-5252 (2015).

44 Bell, R. A. V. *et al.* Chromatin reorganization during myoblast differentiation involves the caspase-dependent removal of SATB2. *bioRxiv* (2019).

**Fig. 1** | Caspases proteolyze peripheral Nups during myogenesis (+ **Extended Data Fig. 1**)

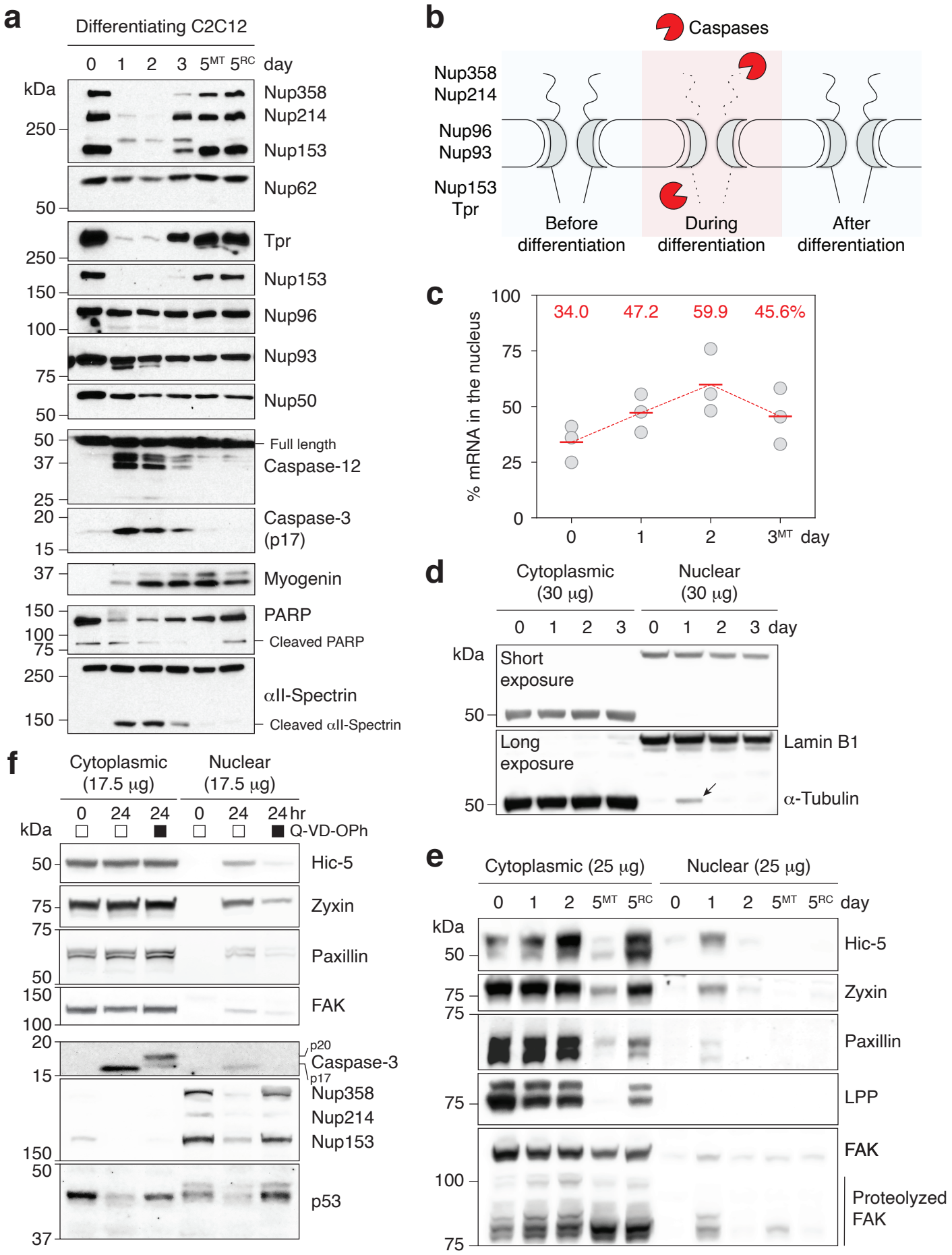

**Fig. 2** | Transient nuclear retention of FAK resets MBD2-mediated genome regulation during myogenesis (+ **Extended Data Fig. 2-4**)

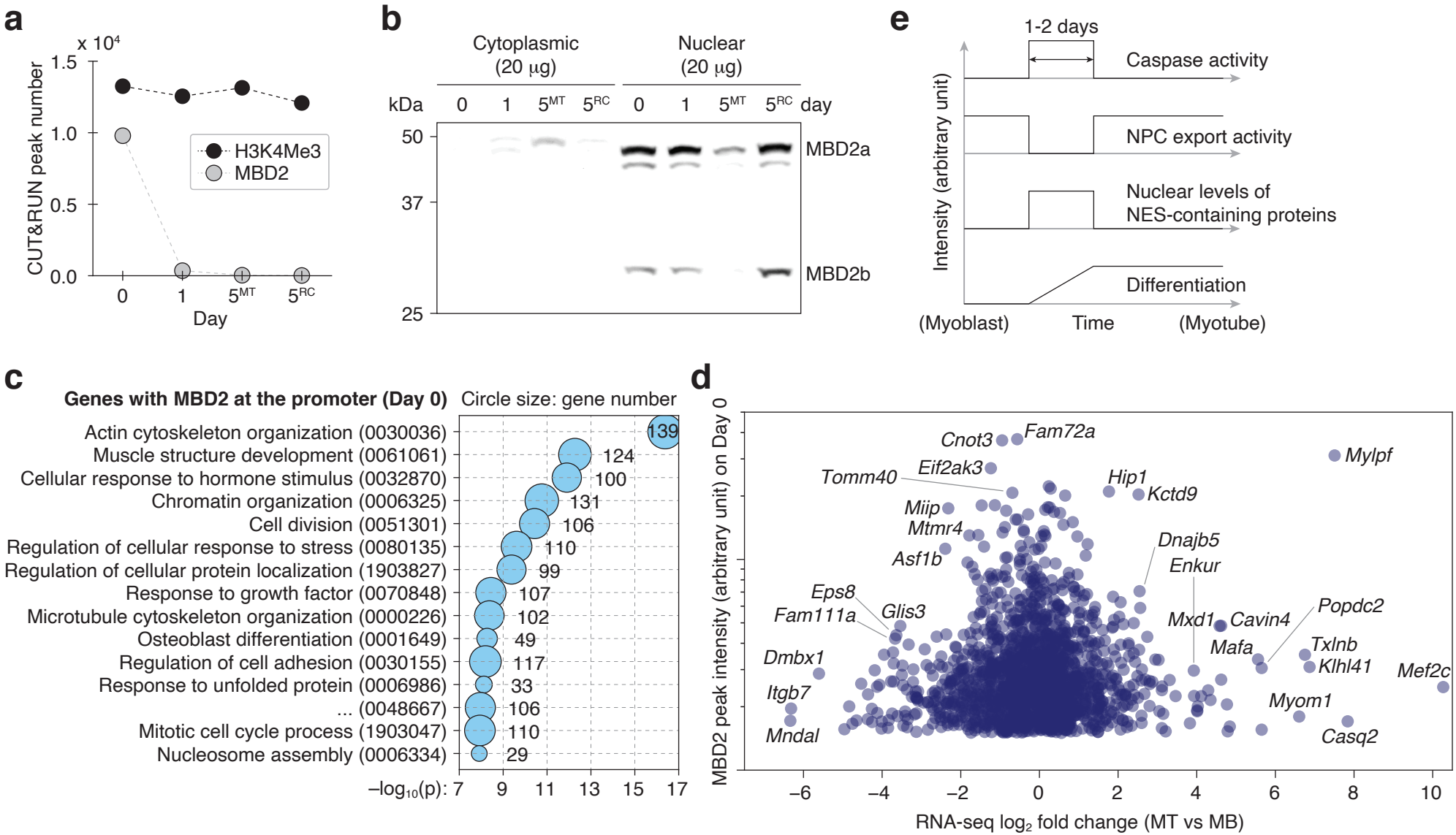

**Fig. 3** | Caspase activation integrates multiple pathways for myogenin upregulation (+ **Extended Data Fig. 5**)

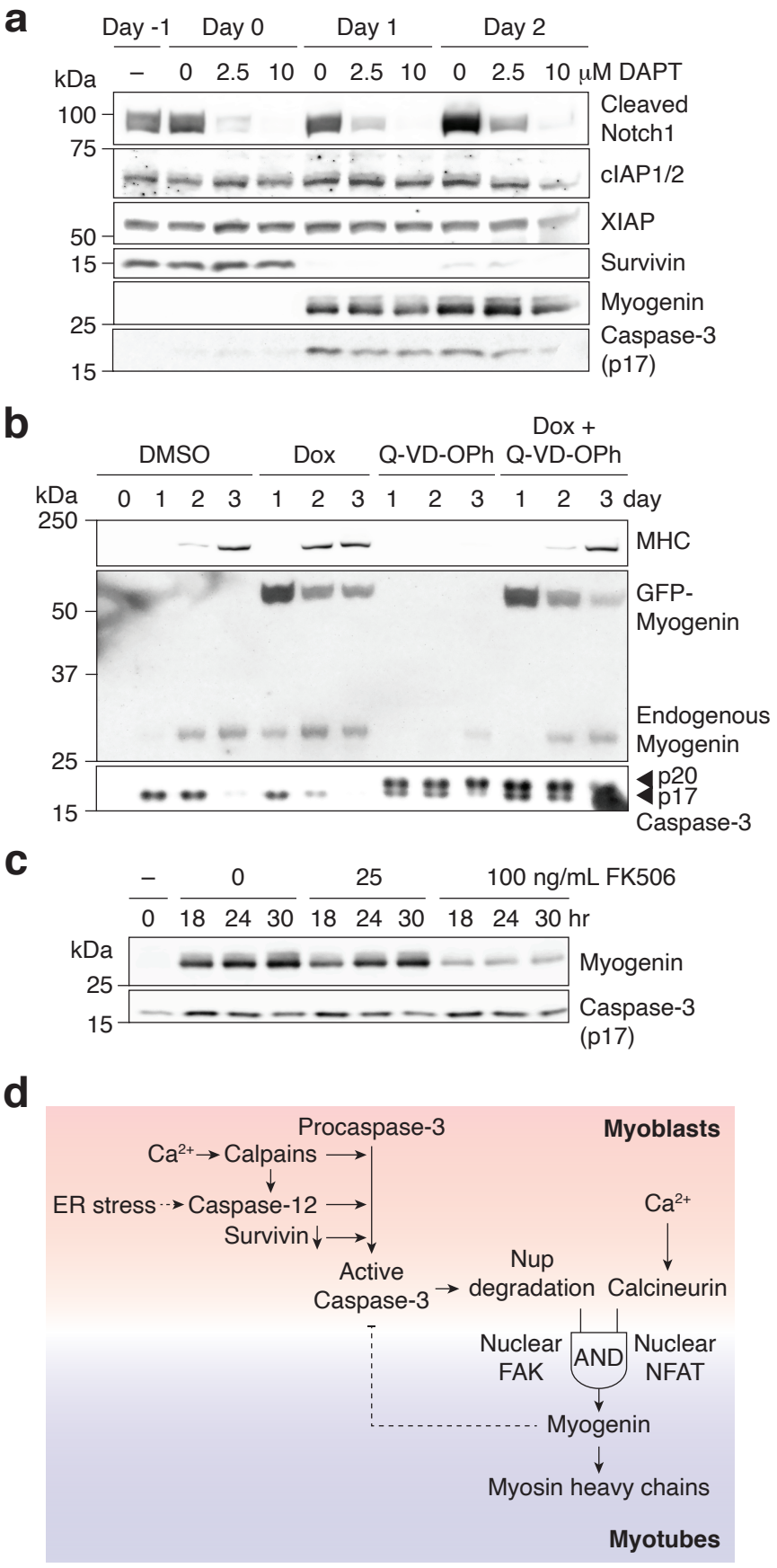

**Fig. 4** | Caspase-mediated NPC trimming occurs during neurogenesis and ER stress

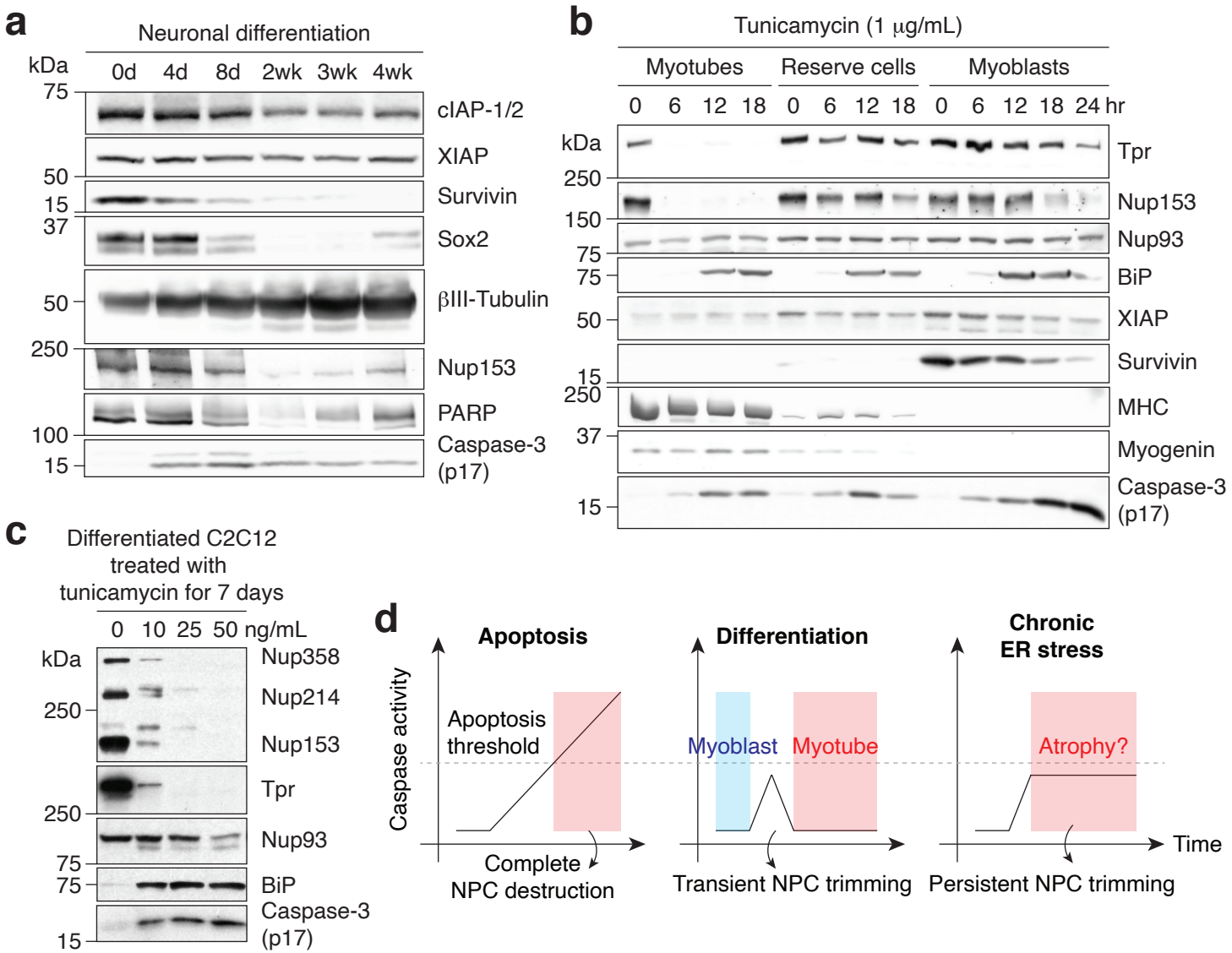

## Figure Legends

**Figure 1 | Caspases proteolyze peripheral Nups during myogenesis. a,** Immunoblots showing the degradation of Nups, PARP, and αII-spectrin, the proteolytic activation of caspase-3 and -12, and the upregulation of myogenin in differentiating C2C12. MT: myotubes, RC: reserve cells. **b,** Schematic representation of caspase-mediated NPC trimming during myogenic differentiation. **c,** Nuclear-to-total mRNA ratio in C2C12 cells undergoing myoblast-to-myotube transition. In red is the average value of three replicates from each point. **d,** Localization of lamin B1 and α-tubulin in differentiating C2C12 cells was assessed by immunoblotting. Nuclear α-tubulin is marked with an arrow. 30 μg of protein from cytoplasmic or nuclear lysate was loaded to each lane. **e,** Cytoplasmic and nuclear levels of NES-containing focal adhesion proteins in differentiating C2C12 cells were assessed by immunoblotting. For both cytoplasmic and nuclear fractions, 25 μg of protein was loaded per lane. **f,** C2C12 cells were differentiated in the absence or presence of a pan-caspase inhibitor, Q-VD-Oph (30 μM) for 24 hours, and nuclear and cytoplasmic fractions were obtained. Nuclear accumulation of NES-containing focal adhesion proteins, caspase-mediated NPC trimming, and p53 degradation were examined by western blotting. 17.5 μg of cytoplasmic or nuclear protein was loaded per lane.

**Figure 2 | Transient nuclear retention of FAK resets MBD2-mediated genome regulation during myogenesis. a,** The number of MBD2 and H3K4Me3 CUT&RUN peaks in differentiating C2C12 cells. **b,** Cytoplasmic and nuclear levels of MBD2 in differentiating C2C12 cells were determined by western blotting. 20 μg of protein was loaded per lane. **c,** GO analysis of the genes whose promoters are bound with MBD2 in confluent myoblasts (day 0). In parentheses are seven-digit GO IDs. GO ID 0048667 corresponds to “cell morphogenesis involved in neuron differentiation”. **d,** Transcriptional changes after MBD2 is removed from the promoter of respective genes. Y-axis denotes MBD2 CUT&RUN peak intensity in confluent myoblasts (day 0). **e,** Schematic representation of caspase activation and downstream events that take place during myogenesis.

**Figure 3 | Caspase activation integrates multiple pathways for myogenin upregulation. a,** Immunoblots showing the expression levels of cleaved Notch1, caspase-inhibiting proteins (cIAP1/2, XIAP, and survivin), myogenin, and active caspase-3 (p17) in C2C12 cells. DAPT was added at 0, 2.5, or 10 μM on day -1, and maintained throughout differentiation. **b,** C2C12 stable

cell line that expresses GFP-myogenin in a doxycycline-dependent manner was differentiated in the absence or presence of 0.5 μM doxycycline and/or 30 μM Q-VD-OPh. Myosin heavy chain (MHC), exogenous and endogenous myogenin, and caspase-3 (active p17 and inactive p20) levels were determined by immunoblotting. **c,** Upregulation of myogenin and formation of caspase-3 p17 were evaluated in the presence of 0, 25, or 100 ng/mL FK506 by immunoblotting. **d,** A working model for caspase activation, peripheral Nup degradation, and myogenin upregulation during myoblast-to-myotube conversion.

**Figure 4 | Caspase-mediated NPC trimming occurs during neurogenesis and ER stress. a,** Expression levels of caspase-inhibiting proteins (cIAP-1/2, XIAP, survivin), neuronal differentiation markers (Sox2 and βIII-tubulin), caspase substrates (Nup153 and PARP), and active caspase-3 (p17) in differentiating neurons were determined by western blotting. **b,** Acute ER stress was induced using 1 μg/mL tunicamycin in C2C12 myotubes, reserve cells, and myoblasts, and the levels of Nups, BiP, caspase-inhibiting proteins (cIAP-1/2 and XIAP), myosin heavy chain (MHC), myogenin, and active caspase-3 (p17) were monitored by immunoblotting. **c,** Chronic ER stress was induced in differentiated C2C12 cells for 7 days using low doses of tunicamycin (0, 10, 25, or 50 ng/mL). The integrity of Nups and the induction of BiP and active caspase-3 (p17) were assessed by immunoblotting. **d,** Schematic representation illustrating caspase activation and NPC proteolysis patterns in apoptosis, cell differentiation, and ER stress.

## Methods

**Antibodies and chemicals.** Primary and secondary antibodies and chemicals used in this study are summarized in **Supplementary Table 2, 3, and 4**.

**Immunoblot techniques.** Cultured cells were washed with phosphate-buffered saline (PBS) and harvested by trypsinization. Cell pellet was washed with PBS, and lysed in RIPA buffer (50 mM Tris-HCl pH 7.5, 150 mM NaCl, 1% Triton X100, 0.5% sodium deoxycholate, 0.1% sodium dodecyl sulfate) containing protease and phosphatase inhibitors (Pierce Protease Inhibitor Mini Tablet, EDTA-free, Thermo Scientific; PhosSTOP, Roche) for 45 minutes at 4ºC. Insoluble material was pelleted at 16,000 x g at 4ºC for 20 minutes. 15-30 μg of total protein per sample were added 6x Laemmli sample buffer, boiled for 4 minutes, and loaded on a Tris or Bis-tris gel for electrophoresis. Proteins were transferred to a nitrocellulose membrane and stained with Ponceau S solution to confirm equal protein loading and successful transfer. After washing with Tris-buffered saline containing 0.05% (w/v) Tween 20 (TBST) several times, the membrane was blocked with 5% non-fat milk power in TBST for an hour at room temperature, and subsequently immunoblotted at 4ºC overnight with primary antibodies listed in **Supplementary Table 2**. Chemiluminescent detection was conducted using either SuperSignal West Pico or Femto kits (Thermo Scientific) after 45-minute incubation with secondary antibodies listed in **Supplementary Table 3** at room temperature. Western blot images were obtained using KwikQuant Imager (Kindle Biosciences) or Odyssey CLx (LI-COR).

**Cloning.** Vectors, PCR templates, and PCR primers used in this study are listed in **Supplementary Table 5**. In-fusion cloning was performed using the In-Fusion HD EcoDry Cloning Plus kit (Takara), and standard cut-and-paste cloning using T7 DNA ligase (New England Biolabs).

**Cell culture.** C2C12 and HCT116 cells were obtained from ATCC. C2C12 cells were cultured in Dulbecco's Modified Eagle Medium (DMEM) supplemented with 20% fetal bovine serum and penicillin-streptomycin. For myogenic differentiation, they were grown to confluency, washed with PBS twice, and added DMEM with 2% horse serum and the same antibiotics. C2C12 differentiation medium was replenished every 24 or 48 hours. After 120 hours, mature myotubes and reserve cells were obtained. Myotubes were harvested with minimal contamination of reserve cells by mild trypsinization (1:3 or 1:4 dilution of trypsin in PBS). HCT116 cells were cultured in

McCoy's 5A Medium supplemented with 10% fetal bovine serum and penicillin-streptomycin. H9 embryonic stem cells were differentiated to neural precursor cells using a previously published method[45]. Purified neural precursor cells were cultured in neurogenic conditions (DMEM/F12 based medium with 1x N2, 1x B27, 20ng/mL GDNF, 20ng/mL BDNF, 1mM cAMP, and 200nM ascorbic acid) for 4 weeks to generate mature post-mitotic neurons.

**C2C12 cell fractionation.** Cells were harvested by trypsinization, washed with PBS, and chilled on ice. Cells were then lysed in ice-cold 0.1% NP40 in PBS, and rotated at 4ºC for 10 minutes. Nuclei were pelleted by centrifugation at 500 x g at 4ºC for 4 minutes, and the supernatant (cytoplasmic fraction) was transferred to a fresh tube and stored at -80ºC until use. Nuclei were again resuspended in ice-cold 0.1% NP40 in PBS, rotated at 4ºC for 5 minutes, and pelleted at 500 x g at 4ºC for 4 minutes. The supernatant was discarded, and the pellet (nuclear fraction) was stored at -80ºC until use.

**Lentivirus packaging, infection, and selection.** Third-generation lentiviral protocol was followed to produced virus in HEK293T cells (obtained from the Salk Stem Cell Core Facility). C2C12 cells were infected with viral supernatant at 30-40% confluency in the presence of 6 μg/mL polybrene for 24 hours, and selected 24 hours after infection with 1 mg/mL puromycin.

**RNA fluorescence *in situ* hybridization (FISH).** C2C12 cells were grown on a No. 1.5 coverslip placed in a 12-well cell culture plate. After removing media, cells were washed with PBS, and fixed in 3.7% paraformaldehyde in PBS for 10 minutes at room temperature. Fixed cells were washed with PBS twice and permeabilized in 70% (vol/vol) ethanol at 4ºC for at least a day. We then followed Stellaris RNA FISH protocol for adherent cells (https://www.biosearchtech.com/support/resources/stellaris-protocols) to fluorescently visualize RNAs. Fluorescent images were obtained using a Leica SP8 confocal microscope equipped with a 63x oil-immersion objective. Images were cropped and pseudocolored using FIJI. See **Supplementary Table 6** for RNA FISH probes used in this study.

**Immunofluorescence.** C2C12 cells were grown on a chambered cell culture slide (Ibidi). Cells were fixed in PBS containing 2% paraformaldehyde for 10 minutes at room temperature, and washed with PBS 3 times. Fixed cells were permeabilized and blocked in immunofluorescence buffer (PBS containing 0.1% Triton-X, 0.02% sodium dodecyl sulfate, and 10 mg/mL bovine serum albumin) for 30 minutes. The cells were then incubated with primary antibodies diluted in

immunofluorescence buffer at room temperature for 2 hours, washed 3 times with immunofluorescence buffer, and incubated with the appropriate secondary antibodies diluted in immunofluorescence buffer at room temperature for 45 minutes. Finally, the cells were washed with immunofluorescence buffer 3 times, and added VECTASHIELD antifade mounting medium with DAPI (Vector Laboratories).Fluorescent images were obtained using a Leica SP8 confocal microscope equipped with a 63x oil-immersion objective. Images were cropped and pseudocolored using FIJI. See **Supplementary Table 2 and 3** for antibodies used for immunofluorescence.

**Poly(A)$^+$ RNA quantification.** Poly(A)$^+$ RNA was isolated from nuclei and whole cells (see C2C12 cell fractionation above) using the Magnetic mRNA Isolation Kit (New England Biolabs). Two rounds of binding, washing, and elution were performed. Eluted RNA was quantified via Qubit RNA HS Assay (Invitrogen).

**MBD2 CUT&RUN-sequencing.** 300-400 thousand cells were used for each CUT&RUN-sequencing reaction. C2C12 cells were harvested by trypsinization, washed in PBS, and stored in fetal bovine serum supplemented with 10% dimethyl sulfoxide until use. MBD2-bound genomic fragments were prepared using the CUT&RUN assay kit (Cell Signaling Technology, 86652). MBD2 antibody (Sigma, M7318) was used at 10 μg/mL. Sequencing libraries were prepared using NEBNext Ultra II DNA library prep kit for Illumina and NEBNext Multiplex Oligos for Illumina (New England Biolabs, E7645 and E7600). Libraries were quantified and analyzed using Qubit dsDNA HS assay kit (Thermo Fisher Scientific) and a TapeStation 2200 with high-sensitivity DNA kit (Agilent). Libraries were sequenced in paired-end 150 base pair mode on the Illumina NovaSeq 6000 platform. Paired-end fragments were trimmed, mapped to the mm10 genome, and filtered using Trim Galore (https://github.com/FelixKrueger/TrimGalore), Bowtie2[46], and SAMtools[47], respectively. Peaks were identified using MACS2[48] and further filtered and analyzed with in-house Python scripts that leveraged pyBigWig (https://github.com/deeptools/pyBigWig) and pyBedTools[49] packages. GO term analyses (biological processes) were performed on http://metascape.org[50]. Genomic annotation of the peaks was conducted using ChIPseeker[51]. CUT&RUN-sequencing data were plotted using karyoploteR[52].

**mRNA-sequencing.** 1-2 million C2C12 cells were lysed in 1 ml TRIzol. 0.4 ml chloroform was added and vigorously shaken for RNA extraction. The aqueous phase was transferred to a fresh tube, and one volume of 70% ethanol was added dropwise while vortexing at the lowest speed at

room temperature. The mixture was purified using RNeasy Mini kit (Qiagen) to yield several hundred ng/μL total RNA. mRNA-sequencing was performed in paired-end 150 base pair mode on the Illumina NovaSeq 6000 platform. Paired-end fragments were mapped to mm10, filtered, and assembled into transcripts using HISAT2[53], SAMtools[47], and StringTie[54]. Differential expression was evaluated using DESeq2[55], and further analyzed with in-house python scripts.

## References


45 Marchetto, M. C. *et al.* Altered proliferation and networks in neural cells derived from idiopathic autistic individuals. *Mol Psychiatry* **22**, 820-835 (2017).

46 Langmead, B. & Salzberg, S. L. Fast gapped-read alignment with Bowtie 2. *Nat Methods* **9**, 357-359 (2012).

47 Li, H. *et al.* The Sequence Alignment/Map format and SAMtools. *Bioinformatics* **25**, 2078-2079 (2009).

48 Zhang, Y. *et al.* Model-based analysis of ChIP-Seq (MACS). *Genome Biol* **9**, R137 (2008).

49 Dale, R. K., Pedersen, B. S. & Quinlan, A. R. Pybedtools: a flexible Python library for manipulating genomic datasets and annotations. *Bioinformatics* **27**, 3423-3424 (2011).

50 Zhou, Y. *et al.* Metascape provides a biologist-oriented resource for the analysis of systems-level datasets. *Nat Commun* **10**, 1523 (2019).

51 Yu, G., Wang, L. G. & He, Q. Y. ChIPseeker: an R/Bioconductor package for ChIP peak annotation, comparison and visualization. *Bioinformatics* **31**, 2382-2383 (2015).

52 Gel, B. & Serra, E. karyoploteR: an R/Bioconductor package to plot customizable genomes displaying arbitrary data. *Bioinformatics* **33**, 3088-3090 (2017).

53 Kim, D., Paggi, J. M., Park, C., Bennett, C. & Salzberg, S. L. Graph-based genome alignment and genotyping with HISAT2 and HISAT-genotype. *Nat Biotechnol* **37**, 907-915 (2019).

54 Pertea, M. *et al.* StringTie enables improved reconstruction of a transcriptome from RNA-seq reads. *Nat Biotechnol* **33**, 290-295 (2015).

55 Love, M. I., Huber, W. & Anders, S. Moderated estimation of fold change and dispersion for RNA-seq data with DESeq2. *Genome Biol* **15**, 550 (2014).